# The structure of the rare-earth phosphate glass $(Sm_2O_3)_{0.205}(P_2O_5)_{0.795}$ studied by anomalous dispersion neutron diffraction



2007 J. Phys.: Condens. Matter 19 056002

(http://iopscience.iop.org/0953-8984/19/5/056002)

INSTITUTE OF PHYSICS PUBLISHING JOURNAL OF PHYSICS: CONDENSED MATTER

J. Phys.: Condens. Matter **19** (2007) 056002 (12pp) doi:10.1088/0953-8984/19/5/056002

# The structure of the rare-earth phosphate glass $(Sm_2O_3)_{0.205}(P_2O_5)_{0.795}$ studied by anomalous dispersion neutron diffraction

**Jacqueline M Cole[1,6], Adrian C Wright[2], Robert J Newport[3], Roger N Sinclair[2], Henry E Fischer[4], Gabriel J Cuello[4] and Richard A Martin[5]**

[1] Department of Physics, University of Cambridge, J J Thomson Avenue, Cambridge CB3 0HE, UK
[2] J J Thomson Physical Laboratory, University of Reading, Whiteknights, Reading RG6 6AF, UK
[3] School of Physical Sciences, Ingram Building, University of Kent, Canterbury CT2 7NH, UK
[4] Institut Laue-Langevin, 6, Rue Jules Horowitz, BP 156, 38042 Grenoble Cedex 9, France
[5] Department of Physics, University of Bath, Claverton Down, Bath BA2 7AY, UK

E-mail: jmc61@cam.ac.uk

Received 15 July 2006, in final form 25 November 2006
Published 15 January 2007
Online at stacks.iop.org/JPhysCM/19/056002

**Abstract**

The role of the $Sm^{3+}$ ions in the structure of vitreous $Sm_2O_3{\cdot}4P_2O_5$ has been investigated using the neutron diffraction anomalous dispersion technique, which employs the wavelength dependence of the real and imaginary parts of the neutron scattering length close to an absorption resonance. The data described here represent the first successful complete neutron anomalous dispersion study on an amorphous material. This experimental methodology permits one to determine exclusively the closest Sm $\cdots$ Sm separation. Knowledge of the R $\cdots$ R (R = rare-earth) pairwise correlation is key to understanding the optical and magnetic properties of rare-earth phosphate glasses. The anomalous difference correlation function, $\Delta T''(r)$, shows a dominant feature pertaining to a Sm $\cdots$ Sm separation, centred at 4.8 Å. The substantial width and marked asymmetry of this peak indicates that the minimum approach of $Sm^{3+}$ ions could be as close as 4 Å. Information on other pairwise correlations is also revealed via analysis of $T(r)$ and $\Delta T(r)$ correlation functions: $Sm^{3+}$ ions display an average co-ordination number, $n_{Sm(O)}$, of 7, with a mean Sm–O bond length of 2.375(5) Å whilst the $PO_4$ tetrahedra have a mean P–O bond length of 1.538(2) Å. Second- and third-neighbour correlations are also identified. These results corroborate previous findings. Such consistency lends support to the application of the anomalous dispersion technique to determine Sm $\cdots$ Sm separations.

(Some figures in this article are in colour only in the electronic version)

[6] Address for correspondence: St Catharine's College, Cambridge CB2 1RL, UK.

## 1. Introduction

Rare-earth (R) phosphate glasses with compositions in the metaphospate–ultraphosphate region $(R_2O_3)_{0.25}(P_2O_5)_{0.75}$–$(R_2O_3)_{0.166}(P_2O_5)_{0.833}$ have shown great promise in the laser and optoelectronics industry. Indeed, these materials have recently been under investigation for commercial application as fibre lasers [1]. This is because the rare-earth ions possess the required energy levels for achieving successful population inversion, and the non-linear refractive index is large enough to exhibit the desired optical effects, without causing beam breakup and damage. Moreover, the particularly high concentration of rare-earth dopant present in these materials results in a myriad of exotic physical properties at low temperatures: negative thermal expansion and pressure dependence of bulk moduli [2] and unprecedented magnetic, magneto-optical and opto-acoustic phenomena [3].

The structural nature of these glasses dictates their physical properties, especially the closest R···R approach, since too close a separation impairs their optical and magnetic phenomena. Conventional x-ray [4–8] and neutron [7, 9] diffraction, EXAFS [4, 10–12], XANES [13] and solid-state NMR [6, 9] studies on glasses, $(R_2O_3)_x(P_2O_5)_{1-x}$, where 0.167 (ultraphosphate) $< x <$ 0.25 (metaphosphate) have, in combination, been able to piece together a model of the local structure out to an interatomic distance, $r$, of about 4 Å (e.g. see figure 5 in [6]). However, the R···R separation is not part of this defined local structure, and beyond this ∼4 Å radial limit these standard characterization techniques are uninformative owing to (i) increasing numbers of overlapping pair-wise correlations in conventional diffraction, making it impossible to deconvolute individual correlations; (ii) the progressively damped signal, and obscuring multiple scattering effects in EXAFS; (iii) the inherent short-range $J$–$J$ coupling effects in NMR, and heavily broadened signal due to the paramagnetic nature of rare-earth ions.

One must resort to using non-conventional diffraction techniques to determine the nearest R···R separation. By exploiting the intrinsic paramagnetism of terbium ions and applying magnetic difference neutron diffraction methods, this goal was recently achieved via a novel and challenging experiment: the first of its kind for an amorphous material [14]. In this case, one was able to isolate R···R correlations exclusively in the terbium phosphate glass, $(Tb_2O_3)_{0.246}(P_2O_5)_{0.722}(Al_2O_3)_{0.032}$, revealing the nearest R···R separation to be 3.9 Å. A second-neighbour R···R separation was also identified, centred at 6.4 Å.

A terbium-based phosphate glass was used specifically for this experiment because it possesses one of the largest magnetic susceptibilities of all rare-earth phosphate glasses that is near-saturated at 4 K, a sample temperature that was accessible within the experiment. For phosphate glasses containing other rare-earth ions, whose magnetic properties are not so favourable for this type of experiment, it can be better to consider exploiting alternative physical characteristics of the ions, and thereby undertaking a different type of non-conventional diffraction experiment, in order to inform us about R···R distances in these materials.

Samarium has a physical characteristic, unique to all rare earths, that makes it ideal for use in a different type of non-conventional diffraction experiment, which yields R···R correlations exclusively in one part, and R···X and X···X correlations (X is any element that is not R) in another part. This is the anomalous neutron dispersion effect associated with the $^{149}$Sm isotope, which is ∼14% naturally abundant in samarium. It is this physical characteristic that we exploit herein. As such, an anomalous dispersion neutron diffraction experiment on vitreous $Sm_2O_3{\cdot}4P_2O_5$ is the subject of this paper.

The anomalous dispersion technique was first suggested for amorphous materials by Krogh-Moe [15] and is employed successfully with x-rays at synchrotron radiation sources, which provide the necessary required incident intensity and sufficiently dynamic energy

spectrum that encompasses the required absorption edge as well as an energy void of all resonant effects. The equivalent neutron technique involves the variation in the neutron scattering length with wavelength around an absorption resonance,

$$b = b^{\circ} + b'(\lambda) + \mathrm{i}b''(\lambda), \tag{1}$$

$b'(\lambda)$ and $b''(\lambda)$ being the wavelength-dependent real and imaginary parts of the scattering length, usually arising from a single isotope of the element in question; $b^{\circ}$ is the wavelength-independent contribution to the scattering length from all of the isotopes present. The relative change in the scattering length for neutrons is very much larger than that in the atomic form-factor for x-rays. This, together with the greatly enhanced cross-section in the region of the absorption resonance, means that it is possible to perform measurements at the peak of the resonance.

The present judicious choice of four wavelength measurements, rather than the two as used previously [16], allows one to exploit both the real and imaginary components of $b_{\mathrm{Sm}}$ in an anomalous dispersion neutron diffraction experiment, such that one can obtain not only a spectrum comprising the Sm $\cdots$ Sm and Sm $\cdots$ X components, but also one comprising the Sm $\cdots$ Sm correlations exclusively. Due to the highly involved technical and analytical nature of this investigation, further technical details of this study are presented in [17]. Therein is also a description of the theory of the method in relation to other experimental diffraction techniques whilst only the theory specific to this experiment is explained here.

## 2. Theory

The total correlation function, $T(r)$, may be written

$$T(r) = \sum_i \sum_j b_i b_j t_{ij}(r), \tag{2}$$

where $t_{ij}(r)$ is the experimentally broadened component of the correlation function and the $i$ summation is taken over all atoms in the composition unit and that for $j$ over all elemental types. Separating out the terms for a particular element A gives

$$T(r) = x_{\mathrm{A}} b_{\mathrm{A}}^2 t_{\mathrm{AA}}(r) + 2x_{\mathrm{A}} b_{\mathrm{A}} \sum_{j \neq A} b_j t_{Aj}(r) + \sum_{i \neq A} \sum_{j \neq A} b_i b_j t_{ij}(r), \tag{3}$$

where $x_{\mathrm{A}}$ is the fraction of A atoms in the composition unit.

If element A has an absorption resonance, within the range of neutron wavelengths amenable to diffraction experiments on amorphous materials, $b_{\mathrm{A}}$ now takes the form given in equation (1) and the experimentally measured correlation function becomes

$$T(r) = x_{\mathrm{A}}[\{b_{\mathrm{A}}^{\circ} + b'_{\mathrm{A}}(\lambda)\}^2 + (b''_{\mathrm{A}}(\lambda))^2] t_{\mathrm{AA}}(r) + 2x_{\mathrm{A}}\{b_{\mathrm{A}}^{\circ} + b'_{\mathrm{A}}(\lambda)\} \sum_{j \neq A} b_j t_{Aj}(r) + \sum_{i \neq A} \sum_{j \neq A} b_i b_j t_{ij}(r). \tag{4}$$

The choice of the optimum wavelengths for an anomalous dispersion experiment on an amorphous material closely follows that for the solution of the phase problem in crystallography, as discussed by Dale and Willis [18], and involves two first-order differences.

(i) The real part $\{b_{\mathrm{A}}^{\circ} + b'_{\mathrm{A}}(\lambda)\}$ is varied while keeping the imaginary part $\{b''_{\mathrm{A}}(\lambda)\}$ constant, such that the real part has values close to its maximum and minimum to give the maximum variation,

$$\Delta T'(r) = \{b'_{\mathrm{A}}(\lambda_1) - b'_{\mathrm{A}}(\lambda_2)\} \left[ \{2b_{\mathrm{A}}^{\circ} + b'_{\mathrm{A}}(\lambda_1) + b'_{\mathrm{A}}(\lambda_2)\} t_{\mathrm{AA}}(r) + 2 \sum_{j \neq A} b_j t_{Aj}(r) \right] \tag{5}$$

and

$$\Delta T'_X(r) = \{b'_{\rm A}(\lambda_1) - b'_{\rm A}(\lambda_2)\}\Bigg[\sum_{i\neq A}\sum_{j\neq A} b_i b_j t_{ij}(r) - x_{\rm A}\{(b^{\circ}_{\rm A})^2 + b^{\circ}_{\rm A}(b'_{\rm A}(\lambda_1) + b'_{\rm A}(\lambda_2)) + b'_{\rm A}(\lambda_1)b'_{\rm A}(\lambda_2) - (b''_{\rm A}(\lambda))^2\}t_{\rm AA}(r)\Bigg] \tag{6}$$

where $X \neq A$. Since the absorption cross-section, $\sigma^A_{\rm A}$, is proportional to $\lambda b''_{\rm A}(\lambda)$, this means that $\sigma^A_{\rm A}$, and hence the (high) absorption correction, is very similar at the two wavelengths. The difference between these two measurements yields the $\rm A\cdots A + A\cdots X$ components {equation (5)} or $\rm A\cdots A + X\cdots X$ components {equation (6)}.

(ii) The imaginary part is varied while keeping the real part constant, by choosing one wavelength close to the peak of the resonance and the other a long way away, thus yielding only the $\rm A\cdots A$ component,

$$\Delta T''(r) = x_{\rm A}[\{b''_{\rm A}(\lambda_3)\}^2 - b''_{\rm A}(\lambda_4)\}^2]t_{\rm AA}(r). \tag{7}$$

In this formulation, we note the theoretical work of Word and Trammell [19] who discuss conditions where four-body correlation functions should be taken into account. In this case, however, given the fact that the absorption resonance is dominant and so broad that Doppler effects are insignificant, we believe that our assumption of a two-body correlation function is valid. In addition, the fact that the concentration of the resonant isotope is low coupled with the fact that this study concerns an amorphous compound and was undertaken using thermal neutrons, makes somewhat redundant certain considerations of this theory in the context of this paper.

## 3. Experimental procedure

The bulk $(Sm_2O_3)_{0.205}(P_2O_5)_{0.795}$ glass sample was prepared by heating 25 mol% of high purity (99.9%) rare-earth oxide in the presence of excess $P_2O_5$ in an aluminium oxide crucible at a temperature of ∼1550 °C. Full synthetic details are described elsewhere [20]. Gooch and Housego Plc were employed to grind the sample down to a highly uniform thin plate of thickness 0.15 mm. The sample composition was determined by electron probe microanalysis whilst the bulk density measurements ($3199 \pm 10$ kg m$^{-3}$) used the Archimedes principle via a measure of the weight of the sample in both air and water [21], yielding an average number density of $0.068\,87 \pm 0.000\,22$ atoms Å$^{-3}$. A small amount of $Al_2O_3$ (1–2 wt% Al) contaminates the sample, arising from the crucible used in sample preparation; this is regularly detected in conventional x-ray and neutron diffraction experiments [6, 9]. The small quantity, and its characteristic Al–O correlation at 1.8 Å, does not interfere with any of the results obtained here. The contaminant is, however, extremely useful from a materials-centred perspective since it prevents the material from becoming brittle [9].

The measurements associated with the theory described in section 2(i) were undertaken using the D4b diffractometer, at the Institut Laue Langevin, Grenoble, France, at incident wavelengths of 0.78 ($\lambda_1$) and 1.15 Å ($\lambda_2$), whilst those described in section 2(ii) were performed using the upgraded D4 instrument, D4c [22], at wavelengths of 0.90 Å ($\lambda_3$) and 0.45 Å ($\lambda_4$). All measurements were conducted in transmission mode, using a very thin plate sample of dimensions 25 mm × 40 mm × 0.15 mm, fixed at 45° to the incident beam. A further diffraction pattern was measured at $\lambda_{D4} = 0.5$ Å (i.e. far from resonance) for a powder sample in a 5 mm thin-walled cylindrical vanadium can, in order to provide a reference interference function akin to those obtained from previous conventional diffraction studies. For each wavelength

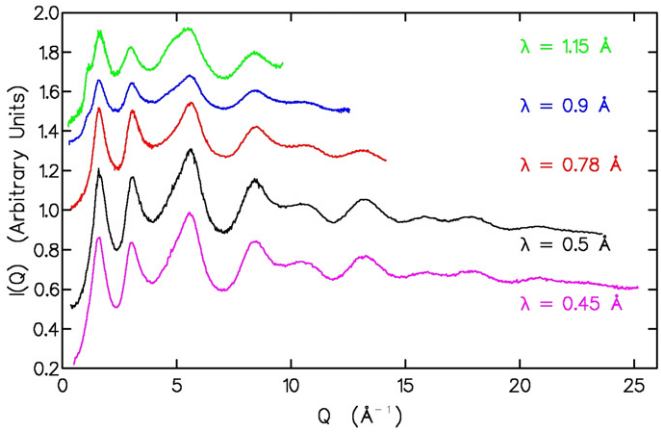


**Figure 1.** The corrected diffraction patterns.

**Table 1.** Neutron scattering lengths, $b$, and cross-sections, $\sigma^S$, for $Sm^{3+}$ for each wavelength used in the measurements.

| | $\lambda$ (Å) | $b^0 + b'(10^{-14}$ m) | $b''(10^{-14}$ m) | $\sigma^S$ (barns) | $Q_{max}$ (Å$^{-1}$) |
|---|---|---|---|---|---|
| $\lambda_3$ | 0.45 | 0.526 | 0.014 | 14.14 | 25.12 |
| $\lambda_{D4}$ | 0.50 | 0.571 | 0.022 | 15.82 | 23.56 |
| $\lambda_1$ | 0.78 | 0.962 | 0.428 | 83.72 | 14.12 |
| $\lambda_4$ | 0.90 | 0.558 | 1.009 | 177.1 | 12.04 |
| $\lambda_2$ ($\sim\lambda_5$) | 1.15 | −0.015 | 0.429 | 81.04 | 9.60 |

measurement, the variation of the real and imaginary parts of the neutron scattering length, $b$, and the cross-section, $\sigma^S$, for natural samarium ($^{Nat}$Sm), is given in table 1. The corresponding $b$ and $\sigma^S$ values for P and O can be considered to be invariant with $\lambda$ in this range and are, respectively, $b = 0.513 \times 10^{-14}$ m, $\sigma^S = 3.312$ barns (P); $b = 0.5803 \times 10^{-14}$ m, $\sigma^S = 4.232$ barns (O) [23].

Supplementary scans on the empty diffractometer, a total absorber ($^{10}B_4C$), and a nickel powder at $\lambda/2$ were also performed in order to make the necessary corrections for the instrumental background, absorption and second-order contamination, respectively. It was also necessary to measure the sample transmission as a function of wavelength and this was done using the time-of-flight instrument, GEM, at ISIS, UK. The data were subsequently corrected for absorption [24, 25] and the final corrected diffraction patterns are compared in figure 1. Cubic-spline fits were performed to each corrected diffraction pattern to yield a constant $Q$ interval, $\Delta Q = 0.02$ Å$^{-1}$. In subtracting off the self-scattering and the paramagnetic scattering from the $Sm^{3+}$ ions [26], to calculate the interference function, $Qi(Q)$, an additional correction was required for a small amount of 'water' contamination (0.29%). This correction was obtained using the water cross-section data of Beyster [27], which were interpolated to the present experimental wavelengths. The same amount of water was assumed for each sample/wavelength. The diffraction patterns were then normalized to the combined self + paramagnetic + 'water' scattering using the Krogh-Moe [28]–Norman [29] technique. In the case of the cylindrical sample ($\lambda = 0.5$ Å), it was also necessary to correct the diffraction pattern for multiple scattering [25] before this normalization. Extended experimental details are given in [17].

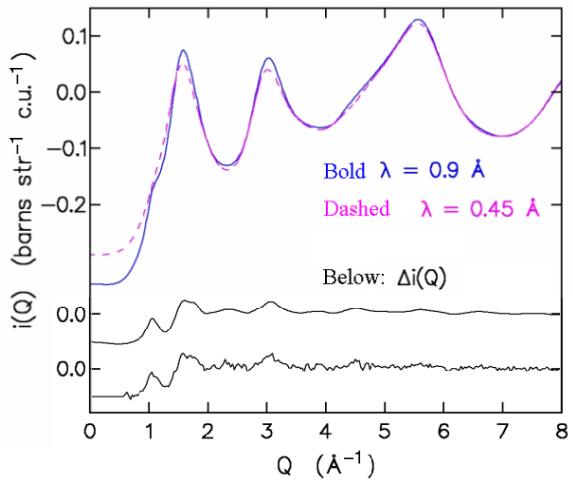


**Figure 2.** The distinct scattering $i(Q)$ obtained at wavelengths of 0.9 and 0.45 Å (top; cubic spline fits), together with the difference, $\Delta i''(Q)$, as calculated from the cubic spline fits (centre) and from the binned raw data points (bottom). One should note that the cubic spline fitting process has almost no effect on the experimental noise in the transform below 10 Å since, at the raw data spacing employed in our work, the Fourier noise components removed are of high frequency and therefore contribute at higher $r$ [30]. The difference correlation functions obtained from these two methods agree within the line thickness of the plots presented here, as shown in detail in the related technical paper [17].

## 4. Results

A comprehensive presentation of the data analysis methods that lead to the primary results given here is described in [17], but to illustrate the significant differences observed in this experiment figure 2 shows the interference functions at $\lambda = 0.45$ and 0.90 Å together with the $\Delta i''(Q)$. Fourier transforms were performed on the resulting interference functions using Filon's quadrature [31] and the Lorch modification function [32] and these are illustrated in figure 3. The high quality of the data is evident via the low noise observed below the first true peak in each of these real-space correlation functions; indeed, this noise is so low that it necessitated no correction term whatsoever. In each case, the maximum value of $Q$, $Q_{\max}$, is the largest possible for the given wavelength (table 1). However, to extract the various difference correlation functions, it is necessary to Fourier transform the two data sets involved with the same value of $Q_{\max}$. The variation of the real part, $\Delta T'(r)$, that yields $\mathrm{A}\cdots\mathrm{A} + \mathrm{A}\cdots\mathrm{X}$ pairwise correlations (equation (5)), is summarized in figure 4(b) and the corresponding procedure for the imaginary part, $\Delta T''(r)$, representing $\mathrm{A}\cdots\mathrm{A}$ contributions exclusively, is illustrated in figure 4(c). The contribution of the 0.78 Å data in the extraction of $\Delta T'_X(r)$, that yields $\mathrm{A}\cdots\mathrm{A} + \mathrm{X}\cdots\mathrm{X}$ contributions (equation (6)), turns out to be negligible given that the real part of the $Sm^{3+}$ scattering length ($b^0 + b'$) is very close to zero ($-0.015 \times 10^{-12}$ cm) at 1.15 Å. $\Delta T'_X(r)$ was therefore not considered any further.

A fit [33] to extract the P–O bond length, $r_{\mathrm{P-O}}$, was performed on the $T(r)$ functions derived from data at all five wavelengths. The two most accurate fits (from the 0.45 and 0.5 Å data) yielded an average $r_{\mathrm{PO}}$ value of 1.538(3) Å and an associated $\sigma_{\mathrm{PO}}$ of 0.075(4) Å (figure 4(a)). Fits using the 0.9 and 1.15 Å data yielded root mean square (rms) bond length variations, $\sigma$, that were significantly narrower than those obtained at the shorter wavelengths, which is almost certainly due to the amplitude of the structure in the diffraction patterns being

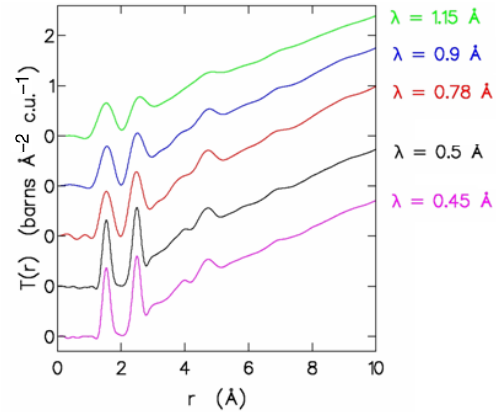


**Figure 3.** The real-space correlation functions, $T(r)$.

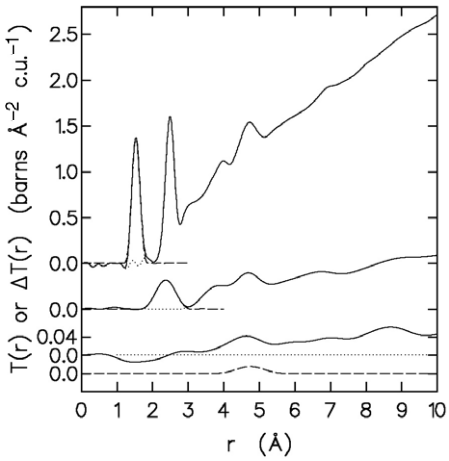


**Figure 4.** (a) $T(r)$ for the 0.45 Å data, together with the fit to the first (P–O) peak (top); (b) $\Delta T'(r)$ plus the fit to the Sm–O peak (middle); (c) $\Delta T''(r)$ together with the simulated peak for Sm $\cdots$ Sm pairs based on a linear Sm–O–Sm arrangement (bottom). For $T(r)$ and $\Delta T'(r)$, the experiment is the solid line, the fit is dashed and the residual dotted. The bottom curves are calculated using a $Q_{\max}$ of 7 Å$^{-1}$ and are scaled by a factor of five; the simulated peak is dashed and the dotted line is zero.

too large at the highest values of $Q$, as a result of uncertainties in the absorption correction. In each case, the P(O) co-ordination number, $n_{\mathrm{P(O)}}$, is four, within the experimental uncertainty. Details of the Sm–O bond length distribution were obtained from a fit to the first peak in $\Delta T'(r)$ (figure 4(b)), giving the values $r_{\mathrm{SmO}} = 2.375(5)$ Å, $n_{\mathrm{Sm(O)}} = 6.9(2)$ and $\sigma_{\mathrm{SmO}} = 0.146(10)$ Å.

## 5. Discussion

Each individual function in figure 3 displays the radial distribution function that one would obtain from a conventional neutron diffraction experiment. They should therefore resemble closely previous neutron diffraction results obtained for this same series of lanthanide phosphate glasses $(R_2O_3)_x(P_2O_5)_{1-x}$ (R = Ce, Ce, Nd, Tb; $x = 0.197$, 0.235, 0.187, 0.263,

respectively) [9]. There, terminal and bridging P–O separations were resolved at 1.49(1) Å and 1.60(1) Å respectively and were present in a 1:1 ratio; R–O separations ranged from 2.27(2) to 2.43(2) Å with sixfold coordination; second-neighbour correlations, O–(P)–O, P–(O)–P and O–(R)–O, were found to exist on average 2.50(1) Å, 3.01(4) Å and 3.23(3) Å apart, respectively; one third-neighbour correlation, P–(OP)–O, was also found to be centred between 2.78 and 2.86(3) Å.

The mean P–O bond length of 1.538(2) Å obtained from this study is identical to the mean of the terminal and bridging distances for these glasses described above, within experimental error. The average bond-length obtained in this study also agrees very well with the mean P–O bond length in crystalline $SmP_5O_{14}$ (1.536 Å) [34]. The coordination number, $n_{PO} = 4$, is well defined, whilst the associated rms bond length variation is identical to that obtained previously for these glasses [9].

The second peak in the correlation functions of figure 3 arises mostly from a combination of Sm–O and O–(P)–O contributions. The O–(P)–O correlation is the major component of this peak since oxygen is much more abundant than Sm in this glass. Modelling the minor Sm–O component, using this peak, can therefore only result in rather poorly defined information about this correlation. However, the Sm–O correlation can be isolated exclusively by the calculation of $\Delta T(r)$ (figure 4(b)) since this affords only Sm $\cdots$ X and Sm $\cdots$ Sm correlations, and Sm–O is the shortest of these by a wide margin, the Sm–(O)–P correlation being the next shortest feature, expected at 3.7 Å. Moreover, Sm–O separations in these materials are difficult to obtain very reliably by conventional diffraction studies since resolution is always compromised due to the overlapping peak that arises from the O–P–O pair correlation [6, 9].

This is therefore a far more favourable situation and the corresponding fit to this first peak in $\Delta T'(r)$ (figure 4) yields a mean Sm–O bond length of 2.375(5) Å. This distance lies comfortably within the range of R–O separations described above for these glasses. The associated rms deviation of 0.146(10) Å, and the average Sm(O) co-ordination number of 6.9(2), however, are both slightly larger than the neutron diffraction results obtained previously for similar sized ions in this series of glasses: sixfold coordination and an rms deviation, $\sigma$, of no more than 0.122(4) Å ($\sigma^2 = 0.015(2)$ Å$^2$ [9]). Given the complete isolation of the Sm–O peak in this study from any other correlations, in contrast to the previous conventional neutron diffraction work, one would expect this study to afford more accurate results. Indeed, this expectation is corroborated by the excellent agreement of these parameters with those from complementary x-ray diffraction (XRD) [6], L-edge [11] and K-edge EXAFS [12] results on $(Sm_2O_3)_x(P_2O_5)_{1-x}$ glasses of the same composition as that used in this study, within experimental error: $N_{RO} = 6.5(6)$ (XRD), 6.9(3) (L-edge EXAFS), 7(1) (K-edge EXAFS); $\sigma_{RO} = 0.100(6)$ Å (XRD), 0.097(4) Å (L-edge EXAFS), 0.074(4) Å (K-edge EXAFS). It is also instructive to remark on the $R_{SmO}$ values obtained from these previous studies: 2.33(2) Å (XRD), 2.32(1) Å (L-edge EXAFS), 2.33(2) Å (K-edge EXAFS); the $R_{SmO}$ obtained by this study is slightly larger, perhaps because, despite the dominant R–O correlations in x-ray diffraction due to the favourable form-factor weighting of $R$, its $R_{RO}$ correlation peak is contaminated by O–(P)–O contributions, whilst the accuracy of the EXAFS results are affected to some extent by multiple scattering and artefacts from Fourier transform termination effects.

Considering the other features in figure 3, P–(OP)–O and O–(R)–O correlations identified in previous neutron diffraction work were not explicitly modelled here, but their contributions are evident from an inspection of the residual, i.e. unmodelled, peak area under the second peak and the feature just above 3 Å. Similarly, the shoulder in $\Delta T'(r)$ (figure 4) rising at $\sim$3.8 Å is not modelled here, but it is known from previous studies that it must result primarily from Sm–(O)–P and Sm–(OP)–O interactions from the $PO_4$ tetrahedra surrounding the Sm(O) co-ordination polyhedron (expected at 3.7 and 4.0–4.1 Å respectively [6]) whilst the peak at

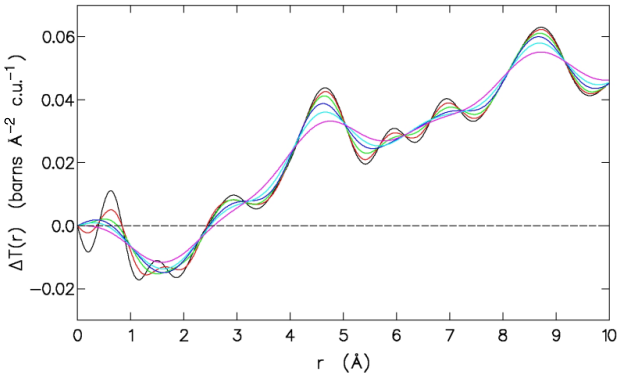


**Figure 5.** The difference correlation function, $\Delta T''(r)$, as derived from the use of different values of $Q_{max}$ (4–9 Å$^{-1}$) in the Fourier transformation. (Pink = 4, cyan = 5, blue = 6, green = 7, red = 8, black = 9 Å$^{-1}$.)

4.7 Å may arise from associated Sm–(2)O distances, conceivably combined with an Sm · · · Sm correlation (see below).

Comparing pairs of diffraction patterns with each other (figure 1), differences can clearly be seen which further indicate the presence of Sm · · · Sm correlations. In particular, a distinct shoulder is present below the first diffraction peak in the 1.15 Å data, whilst it is absent in the 0.78 Å plot. This is certainly not due to resolution effects, because the detailed shape of the second, and especially the third, diffraction peak in each of these patterns also differs. The 0.9 Å diffraction pattern also has a shoulder on the low-$Q$ side of the first peak, but not that recorded at 0.45 Å. This demonstrates that the shoulder is due to the presence of the $Sm^{3+}$ ions and that it must arise from the Sm · · · Sm interactions, since Sm is the only element present with an imaginary contribution to its scattering length.

The measurement of $\Delta T''(r)$ was performed to investigate the distribution of $Sm^{3+}$ ions within the glassy matrix, and in particular the $Sm^{3+} \cdots Sm^{3+}$ inter-ionic distances, which indicate whether the $Sm^{3+}$ ions are distributed randomly, or in more-ordered clusters. The imaginary difference correlation function, $\Delta T''(r)$, is shown on an expanded scale in figure 5 using a variety of $Q_{max}$ values, and, despite the high noise level, appears to have several discernible peaks. The most prominent of these is centred at ∼4.8 Å, which reproduces the feature that appears in $\Delta T'(r)$ to a large extent. The contribution expected for pairs of $Sm^{3+}$ ions with a separation of 4.75 Å, corresponding to linear Sm–O–Sm linkages, with a Sm–Ô–Sm angle of 180° based on twice the R–O separation deduced from $T(r)$ in this study, is entirely consistent with the area under the corresponding peak in $\Delta T''(r)$ (see figure 4(c)). One can place further credence in this Sm · · · Sm assignment given that the peak in $\Delta T''(r)$ remains centred at 4.8 Å as one varies the $Q_{max}$ used for the Fourier transform of this radial distribution function from 4–9 Å$^{-1}$. However, the peak is rather asymmetric on the low side of $r$, which could be evidence for a more minor Sm · · · Sm pairwise correlation centred closer to 4 Å. This would match well the results from a recent magnetic difference neutron diffraction study on a similar rare-earth phosphate glass where a minimum Tb · · · Tb separation of 3.9 Å was deduced [14]. A second neighbour R · · · R correlation was also found in this recent study, centred at 6.4 Å, but with a very wide distribution. These two experimentally observed distances were also revealed via a complementary molecular dynamics study on a terbium metaphosphate glass [35]. There is evidence here that two Sm · · · Sm peaks may be resolvable

in this same range, centred at 5.9 and 6.9 Å, although one must be a bit circumspect here given the sensitivity towards the $Q_{max}$ value chosen to yield the radial distribution function as well as the low magnitude of each of these two proposed features. A much more dominant peak, centred at 8.8 Å but exhibiting a very wide distribution, can be comfortably assigned to a broad range of overlapping Sm · · · Sm pairwise correlations.

The physical consequences of these results are certain: a random distribution of $Sm^{3+}$ ions, in which it is assumed that the atom centres approximate a random loose packing and exhibit no covalent bonding, would lead to an average nearest Sm · · · Sm separation of ∼6.05 Å and a higher coordination number, which is inconsistent with the present data. Local clustering effects must therefore prevail in this compound. Such clustering effects were similarly found in the aforementioned Tb study [14]. Whilst considering any possible relation between these two studies, however, one must be careful to remember that whilst the ionic sizes of terbium and samarium are similar the stoichiometry is slightly different and, perhaps more importantly, low ionization energy and 4f half-shell stabilization effects, respectively, render a tendency of $Sm^{2+}$ and $Tb^{4+}$ formation in the solid state [36]. Therefore, whilst we anticipate a dominant tripositive ionic state for each rare earth in these glasses, a correlation function that represents Sm · · · Sm contributions exclusively will be sensitive to any minor structural manifestations due to these other possible ionic states, and would make the structures of these two glasses rather different.

## 6. Concluding remarks

It may therefore be summarized that vitreous $(Sm_2O_3)_{0.205}(P_2O_5)_{0.795}$ comprises a mixed network of $SmO_n$ polyhedra and $PO_4$ tetrahedra. The $Sm^{3+}$ ions have an average co-ordination number, $N_{SmO}$, of 7, which corroborates prior complementary x-ray diffraction, L-edge and K-edge EXAFS results. This confirms our previously held knowledge about the basic phosphate network and rare-earth environment; such corroboration is extremely useful for the verification of this study given its complexity. The mean Sm–O bond length is 2.375(5) Å. The ability to draw out Sm · · · X + Sm · · · Sm correlations exclusively via the first-order difference, $\Delta T(r)$, affords excellent accuracy in the determination of these Sm–O correlation parameters; in conventional diffraction, Sm–O and O–(P)–O correlations overlap. The anomalous difference correlation function, $\Delta T''(r)$, suggests that the bulk of $Sm^{3+}$ ions are separated from each other on average ∼4.8 Å apart. By calculations based on the R–O correlation, we have shown that the $\Delta T'(r)$ and $\Delta T''(r)$ results, which yield the main R · · · R peak, are mutually consistent. There is evidence of a closer Sm · · · Sm separation nearer to 4 Å, and other Sm · · · Sm correlations at around 5.9 and 6.9 Å. A peak with a very wide distribution (of nearly 2 Å) is centred at 8.8 Å. The fact that there is clear evidence for Sm · · · Sm correlations below those anticipated for a random distribution of $Sm^{3+}$ ions means that local clusters of $Sm^{3+}$ ions must be present in the structure. This information will help in producing more comprehensive structural models so that one can relate better to the optical and magnetic properties of these materials.

The $T(r)$ results are validated by the accurate modelling of the P–O correlation. They also allow the identification of the other second neighbour correlations, P–(O)–P, O–(Sm)–O and Sm–(O)–P, and the third-neighbour correlations, P–(OP)–O and Sm–(OP)–O, as have been revealed in earlier work on these glasses.

The high level of consistency of the new results presented herein with those from previous neutron diffraction studies, as well as those obtained using complementary structural probes (x-ray diffraction, L-edge and K-edge EXAFS), is comforting. Indeed, the comparison serves to validate the success in applying this anomalous dispersion technique to samarium phosphate glasses and demonstrates the feasibility of neutron anomalous dispersion experiments on other

Sm-based amorphous materials. A more comprehensive review of the technical aspects of this work is presented elsewhere [17].

## Acknowledgments

The authors wish to thank Hugh Perrot for the compositional analysis of the sample by electron microprobe techniques. Miguel Gonzalez and Pierre Palleau from the Institut Laue Langevin (ILL), Grenoble, France, and Cora Fisher and Stuart Clarke from the Universities of Bath and Reading, UK, respectively, are also thanked for their experimental assistance on D4 (ILL), as is Alex Hannon from the ISIS Facility, Oxon, UK, for his experimental help with the sample transmission measurements on GEM (ISIS). The ILL is acknowledged for access to its beamtime and facilities. JMC is indebted to the Royal Society for a University Research Fellowship and St. Catharine's College, Cambridge, for a Senior Research Fellowship.

## References

[1] Martin R A and Knight J C 2006 *IEEE Photon. Technol. Lett.* **18** 574
[2] Ace M, Brennan T, Cankurtaran M, Saunders G A and Zahres H 1998 *Phil. Mag.* B **77** 1633
Mierzejewski A, Saunders G A, Sidek H A A and Bridge B 1988 *J. Non-Cryst. Solids* **104** 323
[3] Carini G, Dangelo G, Tripodo G, Fontana A, Rossi F and Saunders G A 1997 *Europhys. Lett.* **40** 435
[4] Bowron D T, Newport R J, Rainford B D, Saunders G A and Senin H B 1995 *Phys. Rev.* B **51** 5739
[5] Bowron D T, BushnellWye G, Newport R J, Rainford B D and Saunders G A 1996 *J. Phys.: Condens. Matter* **8** 3337
[6] Cole J M, Eck E R H, Mountjoy G, Anderson R, Brennan T, Bushnell-Wye G, Newport R J and Saunders G A 2001 *J. Phys.: Condens. Matter* **13** 4105
[7] Hoppe U, Kranold R, Barz A, Stachel D and Hannon A C 1998 *J. Non-Cryst. Solids* **232–234** 44
[8] Hoppe U, Metwalli E, Brow R K and Neuefeind J 2002 *J. Non-Cryst. Solids* **297** 263
[9] Cole J M, van Eck E R H, Mountjoy G, Newport R J, Brennan T and Saunders G A 1999 *J. Phys.: Condens. Matter* **11** 9165
[10] Bowron D T, Saunders G A, Newport R J, Rainford B D and Senin H B 1996 *Phys. Rev.* B **53** 5268
[11] Anderson R, Brennan T, Cole J M, Mountjoy G, Pickup D M, Newport R J and Saunders G A 1999 *J. Mater. Res.* **14** 4706
[12] Cole J M, Newport R J, Bowron D T, Pettifer R F, Mountjoy G, Brennan T and Saunders G A 2001 *J. Phys.: Condens. Matter* **13** 6659
[13] Mountjoy G, Cole J M, Brennan T, Newport R J, Saunders G A and Wallidge G W 2001 *J. Non-Cryst. Solids* **279** 20
[14] Cole J M, Hannon A C, Martin R A and Newport R J 2006 *Phys. Rev.* B **73** 104210
[15] Krogh-Moe J 1966 *Acta Chem. Scand.* **20** 2890
[16] Wright A C, Etherington G, Erwin Desa J A and Sinclair R N 1982 *J. Physique Coll.* C9 31
[17] Wright A C, Cole J M, Newport R J, Fisher C E, Clarke S J, Sinclair R N, Fischer H E and Cuello G J 2006 *Nucl. Instrum. Meth. Phys. Res.* A at press
[18] Dale D H and Willis B T M 1966 *U.K.A.E.A. Report* AERE-R5195
[19] Word R E and Trammell G T 1981 *Phys. Rev.* B **24** 2430
[20] Mierzejewski A, Saunders G A, Sidek H A A and Bridge B 1988 *J. Non-Cryst. Solids* **104** 323
[21] Brennan T 1998 *PhD Thesis* University of Bath, UK
[22] Fischer H E, Cuello G J, Palleau P, Feltin D, Barnes A C, Badyal Y S and Simonson J M 2002 *J. Appl. Phys.* A **74** S160–2
[23] Sears V F 1992 *Neutron News* **3** 26
[24] Wignall G D 1967 *U.K.A.E.A. Report* AERE-M1928
[25] Johnson P A V, Wright A C and Sinclair R N 1983 *J. Non-Cryst. Solids* **58** 109
[26] Brown P J 2001 *Neutron Data Booklet* ed A-J Dianoux and G Lander (Grenoble: Institut Laue-Langevin) p 2.5-1
[27] Beyster J R 1968 *Nucl. Sci. Eng.* **31** 254
[28] Krogh-Moe J 1956 *Acta Crystallogr.* **9** 951
[29] Norman N 1957 *Acta Crystallogr.* **10** 370
[30] Dixon M, Wright A C and Hutchinson P 1977 *Nucl. Instrum. Methods* **143** 379

[31] Filon L N G 1929 *Proc. R. Soc. (Edinburgh)* **49** 38
[32] Lorch E A 1969 *J. Phys. C: Solid State Phys.* **2** 229
[33] Wright A C 1993 *Experimental Techniques of Glass Science* ed C J Simmons and O H El-Bayoumi (Westerville: American Ceramic Society) p 205
[34] Tranqui P D, Bagieu M and Durif A 1974 *Acta Crystallogr.* B **30** 1751
[35] Clark E B, Mead R N and Mountjoy G 2006 *J. Phys.: Condens. Matter* **18** 6815
[36] Huheey J E 1983 *Inorganic Chemistry: Principles of Structure and Reactivity* 3rd edn, Cambridge, p 798